Determinism and invariant measures for diffusing passive scalars advected by unsteady random shear flows

Lingyun Ding and Richard M. McLaughlin

Determinism and invariant measures for diffusing passive scalars advected by unsteady random shear flows

Lingyun Ding[*] and Richard M. McLaughlin[†]

Department of Mathematics, University of North Carolina, Chapel Hill, NC, 27599, United States
(Dated: November 2021)

We study the long-time behavior of an advection-diffusion equation with a general time-varying (including random) shear flow imposing no-flux boundary conditions on channel walls. We derive the asymptotic approximation of the scalar field at long times by using the center manifold theory. We carefully compare it with existing time-varying homogenization theory as well as other existing center manifold based studies, and present conditions on the flows under which our new approximations give a substantial improvement to these existing theories. A recent study [Ding et al., Physica D, **432**, 133118 (2022)] has shown that Gaussian random shear flows induce a deterministic effective diffusivity at long times, and explicitly calculated the invariant measure. Here, with our established asymptotic expansions, we not only concisely demonstrate those prior conclusions for Gaussian random shear flows, but also generalize the conclusions regarding determinism to a much broader class of random (non-Gaussian) shear flows. Such ergodicity-like results are important since they assure an experimentalist only need to perform a single realization of a random flow to observe the ensemble moment predictions at long times. Monte-Carlo simulations are presented illustrating how the highly random behavior converges to the deterministic limit at long times. Counterintuitively, we present a case demonstrating that the random flow may not induce larger dispersion than its deterministic counterpart, and in turn present rigorous conditions under which a random renewing flow induces a stronger effective diffusivity. Lastly, for white in time flows and renewing flows, we derive the invariant measure and explore its Peclet number dependencies.

Keywords: Passive scalar; Scalar intermittency; Shear dispersion; Random shear flow; Turbulent transport; Ergodicity; Renewing process

1. INTRODUCTION

How fluid motion transports a diffusing scalar is an extremely important class of problems in engineering, chemistry. Since G. I. Taylor [61] first introduced the calculation showing that a steady pressure-driven flow in a pipe leads to a greatly enhanced effective diffusivity, the literature on this topic has exploded in many directions spanning many disciplines. Shortly following G. I. Taylor, Aris [5] presented an alternative approach for shear layers yielding a hierarchy for the spatial moments of the scalar field. More recent moment analysis shows how the boundary geometry of the pipe can be used to control the distribution of solute which is advected by the pressure-driven flow [2–4].

Unsteady flows typically generate different properties than their steady counterparts. Practical examples of unsteady flow include pulsatile blood flows [58] and tidal estuaries [28]. The first investigation of the Taylor dispersion in time-dependent flow dates back to Aris [6], who presented the study of a solute advected by pulsating flow in a circular tube. After that, based on the Aris' moment method, a number of studies reported on the enhanced diffusivity induced by the single-frequency pulsating flow[16, 27, 40, 50, 68], the single frequency Couette-Poiseuille [11–13, 52] and the multi-frequency flow [31, 65, 66]. Alternative approaches, using center manifold theory, [45, 46, 48, 49] or homogenization methods [29, 30, 41] not only predict the effective diffusivity but also give the direct expression for the full concentration field at long times.

In this article, we study three points that have not been addressed well in the literature regarding shear dispersion in time-varying flows. First, most of those theoretical studies focused on the cross-sectional averaged concentration, while fewer studies have explored asymptotic corrections which capture cross-channel variations. Here, with the center manifold theory, we present a systematic procedure to construct an approximation to capture the traverse variation of the scalar field. Second, several interesting articles [45, 48, 49] implemented center manifold theory for such unsteady problems employing certain slowly varying assumptions to simplify the calculation. Such assumptions restrict the applicability of the effective dynamics. Here we relax this assumption by carefully incorporating the

---

*Electronic address: dingly@live.unc.edu
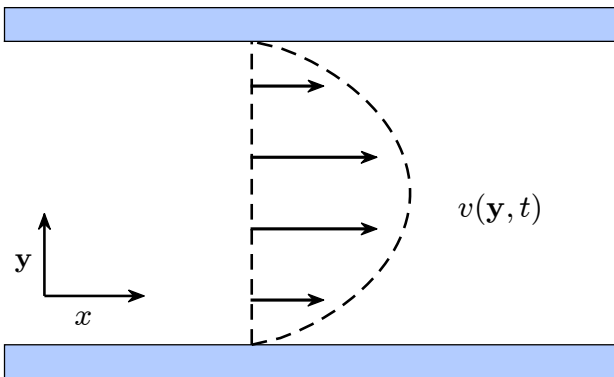†Electronic address: rmm@email.unc.edu; corresponding author

FIG. 1: A schematic of the setup for the special case of a quadratic shear flow.

temporal fluctuation of the flows into the analysis. Hence, our results can handle rapidly fluctuating flows or even random flows. Third, recent results have explicitly calculated using statistical moment closure the invariant measure for a diffusing passive scalar advected by a class of random shear flows [20, 32] employing no-flux boundary conditions on channel domains. These results generalize prior turbulent intermittency in free space of Majda [42] and Kraichnan [44]. Interestingly, we establish here how the center manifold theory can be used to greatly extend these theories to a much broader class of random shear flows, particularly regarding their temporal statistics. We show that for this broader class of flows, all effective diffusion coefficients converge to a deterministic value in the confined domain, in contrast to Majda and others' free-space analog [19, 47], in which the effective diffusion coefficients are random at all times. Such ergodicity-like results assure an experimentalist only needs to perform a single realization of the random flow to observe the field moment predictions at long times.

The paper is organized as follows. In section 2, we formulate the governing equation of the shear dispersion problem and review the Aris moment method. In section 3, we discuss the procedure of applying center manifold theory to the Taylor dispersion problem with time-varying shear flow. By utilizing the first-order approximation for the cross-sectional averaged concentration, we present a nonnegative asymptotic expansion of the scalar field at long times which captures the transverse variations. We document situations in which a time-varying cell problem produces a more accurate approximation than the parametric (adiabatic) approach employed recently [45, 48, 49]. In section 4, we demonstrate that a class of flows with finite correlation time will induce a deterministic effective diffusivity at long times. Moreover, we establish conditions that guarantee that the renewing flow always yields a larger effective diffusivity than its deterministic counterpart. By utilizing the derived new effective equation, we compute the explicit formula of invariant measure of the random passive field.

2. SETUP AND BACKGROUND OF THE PROBLEM

2.1. Governing Equation and Nondimensionalization

Advection-diffusion Equation

We consider the problem in a channel domain $(x, \mathbf{y}) \in \mathbb{R} \times \Omega$, where the x-direction is the longitudinal direction of the channel and $\Omega \subset \mathbb{R}^d$ stands for the cross-section of the channel. Some practical examples of the boundary geometry includes the parallel-plate channel $\Omega = \{y | y \in [0, L]\}$, the circular pipe $\Omega = \{\mathbf{y} | \mathbf{y}^2 \leq L\}$, the rectangular duct $\Omega = \{\mathbf{y} | \mathbf{y} \in [0, L] \times [0, H]\}$, and bowed rectangular channels [43]. As sketched in figure 1, the passive scalar is governed by the advection-diffusion equation with a general time-varying shear flow $v(\mathbf{y}, t)$ and no-flux boundary conditions,

$$\partial_t T + v(\mathbf{y}, t)\partial_x T = \kappa \Delta T, \quad T(x, \mathbf{y}, 0) = T_I(x, \mathbf{y}), \quad \partial_{\mathbf{n}} T|_{\mathbb{R} \times \partial\Omega} = 0, \tag{1}$$

where κ is the diffusivity, $T_I(x, \mathbf{y})$ is the initial data, $\mathbf{n}$ is the outward normal vector of the boundary $\mathbb{R} \times \partial\Omega$ and $\partial\Omega$ is the boundary of Ω.

Nondimensionalization

With the change of variables

$$Lx' = x, \quad L\mathbf{y}' = \mathbf{y}, \quad \frac{L^2}{\kappa}t' = t, \quad Uv'(\mathbf{y}',t') = v(\mathbf{y},t), \quad L\Omega' = \Omega,$$

$$T'_I(x',\mathbf{y}')L^{-d-1} \int_{\mathbb{R}\times\Omega} T_I(x,\mathbf{y})\mathrm{d}x\mathrm{d}\mathbf{y} = T_I(x,\mathbf{y}),$$

$$T'(x',\mathbf{y}',t')L^{-d-1} \int_{\mathbb{R}\times\Omega} T_I(x,\mathbf{y})\mathrm{d}x\mathrm{d}\mathbf{y} = T(x,\mathbf{y},t),$$
(2)

after dropping the primes, we obtain the nondimensionalized advection-diffusion equation

$$\partial_t T + \mathrm{Pe}v(\mathbf{y},t)\partial_x T = \Delta T, \ T(x,\mathbf{y},0) = T_I(x,\mathbf{y}), \quad \partial_{\mathbf{n}} T|_{\mathbb{R}\times\partial\Omega} = 0,$$
(3)

where $\mathrm{Pe} = UL/\kappa$ is the Péclet number.

Variance and skewness

The homogenization method in [21, 31] suggests that, assuming a scale separation in the initial data, the solution of equation (1) can be approximated by a diffusion equation in the longitudinal direction with an effective diffusion coefficient. Inspired by that, we are interested in the variance and skewness of the longitudinal distribution of the scalar field.

The cross-sectional average of the scalar field is defined as $\bar{T}(x,t) = \frac{1}{|\Omega|}\int_\Omega T(x,\mathbf{y},t)\mathrm{d}\mathbf{y}$, where $|\Omega|$ is the area of Ω. In this following context, we use the overline to denote the cross-sectional average. The nth moment of $\bar{T}$ is defined by $\bar{T}_n(t) = \int_{-\infty}^{\infty} x^n \bar{T}(x,t)\mathrm{d}x$. The effective longitudinal effective diffusivity could be computed through the Aris moments

$$\kappa_{\mathrm{eff}} = \lim_{t\to\infty} \frac{\mathrm{Var}(\bar{T})}{2t},$$
(4)

where $\mathrm{Var}(\bar{T}) = \bar{T}_2 - \bar{T}_1^2$ is the variance of the cross-sectional average $\bar{T}$.

The effective diffusivity characterizes the symmetric property of the longitudinal distribution. We are also interested in the asymmetry properties of $\bar{T}$. Skewness is the lowest order integral measure of the asymmetry of a real-valued probability distribution, which is defined as

$$\mathrm{S}(\bar{T}) = \frac{\bar{T}_3 - 3\bar{T}_2\bar{T}_1 + 2\bar{T}_1^3}{\left(\bar{T}_2 - \bar{T}_1^2\right)^{\frac{3}{2}}}.$$
(5)

The information provided by the skewness and how it depends on the tube shape could improve the design of microfluidic flow injection analysis [4, 62] and chromatographic separation [15].

3. CENTER MANIFOLD DESCRIPTION OF THE SHEAR DISPERSION PROBLEM

3.1. Center manifold and reduction principle

In pioneering work, Mercer and Roberts [48] interpreted the long-time asymptotics of the shear dispersion problem as the center manifold of a dynamical system, which provides a systematic and near rigorous approach to derive the approximation. In addition to the shear dispersion problem, practical applications of the center manifold theory include chromatographic model and reactors[10], elastic beam deformations[54], and thin fluid flows dynamics [55, 56]. To explain the center manifold method, we consider an autonomous differential system of the form

$$\frac{\mathrm{d}\mathbf{x}}{\mathrm{d}t} = A\mathbf{x} + f(\mathbf{x},\mathbf{y}), \quad \frac{\mathrm{d}\mathbf{y}}{\mathrm{d}t} = B\mathbf{y} + g(\mathbf{x},\mathbf{y}),$$
(6)

where $\mathbf{x} \in \mathbb{R}^m, \mathbf{y} \in \mathbb{R}^n$. A, B are matrices whose eigenvalues have vanishing and negative real parts, respectively. We also assume $f(\mathbf{x}, \mathbf{y})$, $g(\mathbf{x}, \mathbf{y})$ and their first order partial derivatives are zero at $\mathbf{x} = \mathbf{0}, \mathbf{y} = \mathbf{0}$. These conditions guarantee the existence of a center manifold $\mathbf{y} = h(\mathbf{x})$ which has two important features. First, the stability properties of the dynamical system (6) at the origin are the same as the following lower-dimensional equation

$$\frac{\mathrm{d}\mathbf{x}}{\mathrm{d}t} = A\mathbf{x} + f(\mathbf{x}, h(\mathbf{x})). \tag{7}$$

Second, in the case of a stable equilibrium $(\mathbf{x}, \mathbf{y}) = (\mathbf{0}, \mathbf{0})$, each solution of the system (6) which starts close to the origin exponentially decays to a particular solution on the center manifold [23, 24]. With these two features of the center manifold, one can reduce the original $m + n$-dimensional system (6) to a m-dimensional system (7) with only the price of exponential corrections.

This classical center manifold theory and reduction principle could be generalized in many directions. First, the dynamical system (6) could be an infinite-dimensional system where the matrices A, B become linear operators [25]. Second, similar results hold for a more general dynamical system $\frac{\mathrm{d}\mathbf{x}_i}{\mathrm{d}t} = A_i\mathbf{x}_i + f(\mathbf{x}_1, ..., \mathbf{x}_N, t)$, $1 \leq i \leq N$ and the restriction of eigenvalues could be weakened [8, 63]. This generalization leads to a so-called two-mode invariant manifold model for the shear dispersion problem [60, 69, 70]. Third, more related to our topic, the system could be non-autonomous, where the center manifold becomes time-dependent $\mathbf{y} = h(\mathbf{x}, t)$ [7, 9]. Moreover, the nonlinear term could be discontinuous in t as long as it is strongly measurable with respect to t [9]. A lower bound of the exponential convergence rate is determined by the linear operators, A_i. For further details regarding center manifold theory, we refer to [8, 23] and references therein.

Notice that the advection-diffusion equation (3) is linear, while the center manifold theory applies to a system with nonlinear terms. To apply center manifold theory to the passive scalar problem, we first take the Fourier transform of equation (3) which is defined as $\hat{f}(\mathbf{k}) = (2\pi)^{-\frac{N}{2}} \int_{\mathbb{R}^N} e^{-\mathrm{i}(\mathbf{x}\cdot\mathbf{k})} f(\mathbf{x})\mathrm{d}\mathbf{x}$ and obtain

$$\frac{\partial \hat{T}}{\partial t} - \mathrm{i}k\mathrm{Pe}v(\mathbf{y}, t)\hat{T} = -k^2\hat{T} + \Delta_{\mathbf{y}}\hat{T}, \ \left.\frac{\partial \hat{T}}{\partial \mathbf{n}}\right|_{\mathbb{R}\times\partial\Omega} = 0, \ \hat{T}(k, \mathbf{y}, 0) = \hat{T}_I(k, \mathbf{y}). \tag{8}$$

Second, we conceptually non-linearize equation (8) by treating the wavenumber as a dependent variable of the dynamical system. Notice that $\Delta_{\mathbf{y}}$ has a null space that consists of all functions which are independent of y. To fit the form of equation (6), we rewrite equation (8) as

$$\partial_t \begin{bmatrix} k \\ \hat{\overline{T}} \end{bmatrix} = \begin{bmatrix} 0 & 0 \\ 0 & \Delta_{\mathbf{y}} \end{bmatrix} \begin{bmatrix} k \\ \hat{\overline{T}} \end{bmatrix} + \begin{bmatrix} 0 \\ \overline{\mathrm{i}k\mathrm{Pe}v(\mathbf{y}, t)\hat{T}} - k^2\hat{\overline{T}} \end{bmatrix},$$

$$\partial_t \hat{T}' = \Delta_{\mathbf{y}}\hat{T}' + \mathrm{i}k\mathrm{Pe}v(\mathbf{y}, t)\hat{T} - k^2\hat{T}' - \overline{\mathrm{i}k\mathrm{Pe}v(\mathbf{y}, t)\hat{T}}, \tag{9}$$

$$\left.\frac{\partial \hat{T}}{\partial \mathbf{n}}\right|_{\mathbb{R}\times\partial\Omega} = 0, \quad \hat{T}(k, \mathbf{y}, 0) = \hat{T}_I(k, \mathbf{y}),$$

where $T'(x, \mathbf{y}, t)$ and $\overline{T}(x, t)$ are the fluctuation and average of $T(x, \mathbf{y}, t)$ with respect to $\mathbf{y}$. To weaken the nonlinear coupling, we assume that the initial condition $\hat{T}$ is supported in a neighborhood of $k = 0$, which is the slow varying assumption used in homogenization theory. Then this system satisfies the condition of theorem 2.1 in [9] which guarantees the existence of a center manifold $\hat{T}' = h(\hat{\overline{T}}, k, t)$. Additionally, the solution $\hat{T}$ in the neighborhood of the center manifold converges to $h(\hat{\overline{T}}, k, t) + \hat{\overline{T}}$ exponentially as $t \to \infty$ with the decay rate determined by the diffusion time scale. For nonnegative and integrable initial conditions, due to the diffusion effect, T is a decaying scalar field, in which the energy concentrates near the neighborhood of $k = 0$ at long times. We can seek the expansion of $h(\hat{\overline{T}}, k, t)$ for small k and $\hat{\overline{T}}$, $h = \sum_{n=1}^{\infty} h_n(\mathbf{y}, t)k^n\hat{\overline{T}} + \mathcal{O}(\hat{\overline{T}}^2)$. That is equivalent to approximating the scalar field T by the derivatives of its cross-sectional average $\overline{T}$ with respect to x. This idea dated back to Gill [34, 35] and also has been discussed in [74].

For simplicity, we rewrite all equations in term of physical variables,

$$\partial_t\overline{T} = \partial_x^2\overline{T} - \mathrm{Pe}\overline{v(\mathbf{y}, t)\partial_x T}, \quad \partial_t T = \Delta_{\mathbf{y}}T + \partial_x^2 T - \mathrm{Pe}v(\mathbf{y}, t)\partial_x T. \tag{10}$$

The expansion becomes

$$T = T' + \bar{T} = \bar{T} + h(\bar{T}) = \sum_{n=0}^{\infty} \theta_n(\mathbf{y}, t) \partial_x^n \bar{T}. \tag{11}$$

The fluctuation T' has a zero mean, $\int_{\Omega} T' d\mathbf{y} = 0$, which implies $\bar{\theta}_0 = 1$ and $\bar{\theta}_n = 0$ if $n \geq 1$ at long times. We have $\frac{\partial}{\partial \mathbf{n}} \theta_n \big|_{\mathbf{y} \in \partial \Omega} = 0$ from the no-flux boundary conditions of T. Substituting expansion (11) into equation (10), we have

$$\partial_t \bar{T} = \partial_x^2 \bar{T} - \text{Pe} \overline{v \partial_x T}, \tag{12a}$$

$$\sum_{n=0}^{\infty} \partial_t \theta_n \partial_x^n \bar{T} + \sum_{n=0}^{\infty} \theta_n \partial_x^n \partial_t \bar{T} = \Delta_{\mathbf{y}} T + \partial_x^2 T - \text{Pe} v \partial_x T. \tag{12b}$$

Grouping all terms of the same order, namely $\partial_x^n \bar{T}$, we find that we have to solve the sequence of equations

$$
\begin{aligned}
&(\partial_t - \Delta_{\mathbf{y}}) \theta_0 = 0, \\
&(\partial_t - \Delta_{\mathbf{y}}) \theta_1 = -\text{Pe} \theta_0 \left(v - \overline{\theta_0 v} \right), \\
&(\partial_t - \Delta_{\mathbf{y}}) \theta_n = -\text{Pe} v \theta_{n-1} + \text{Pe} \sum_{m=0}^{n-1} \theta_{n-m-1} \overline{v \theta_m},
\end{aligned}
\tag{13}
$$

where $\theta_n = 0$ if $n < 0$. After solving θ_n successively, we obtain the closed evolution equation of $\bar{T}$ by substituting $T = \sum_{n=0}^{\infty} \theta_n(\mathbf{y}, t) \partial_x^n \bar{T}$ into equation (10),

$$\partial_t \bar{T} = \partial_x^2 \bar{T} - \text{Pe} \sum_{n=0}^{\infty} \overline{v \theta_n} \partial_x^{n+1} T. \tag{14}$$

Finally, once we solve equation (14) for $\bar{T}$, we obtain the approximation of the scalar field T via expansion (11).

3.2. The first and second order effective equation

In this subsection, we will compute equation (13) and (14) for the flow $v(\mathbf{y}, t) = \xi(t) u(\mathbf{y})$. For more general non-separable flow $v(\mathbf{y}, t)$, one could reduce it to a separable form by utilizing the Fourier transform in time. To simplify the calculation, we assume $T_I(x, \mathbf{y}) = \delta(x)$. Otherwise, the general initial condition only creates extra exponential decaying terms and yields the same asymptotic expansion at long times.

With the constraints of the average and boundary conditions of θ_n, we have $\theta_0 = 1$. Therefore, the equation of θ_1 becomes

$$(\partial_t - \Delta_{\mathbf{y}}) \theta_1 = -\text{Pe}(v - \bar{v}), \quad \partial_{\mathbf{n}} \theta_1 \big|_{\partial \Omega} = 0. \tag{15}$$

Since the theory concerns the long time dynamics of the scalar field and the long time limit of θ_1 doesn't depend on the initial condition, in principle, one can solve equation (15) with arbitrary initial condition. To obtain a better approximation at earlier stage, one can choose suitable initial condition of θ_n to match both sides of the expansion (11) at $t = 0$. Then when $v(\mathbf{y}, t) = \xi(t) u(\mathbf{y})$ and $\theta_1(\mathbf{y}, 0) = 0$, the solution of equation (15) is

$$\theta_1(\mathbf{y}, t) = -\text{Pe} \sum_{n=1}^{\infty} \phi_n \langle u, \phi_n \rangle \int_0^t e^{\lambda_n(s-t)} \xi(s) ds. \tag{16}$$

where $\langle f, g \rangle = \frac{1}{|\Omega|} \int_{\Omega} fg \, d\mathbf{y}$. ϕ_n, λ_n are the eigenfunctions and eigenvalues of the Laplace operator in the cross section of the channel Ω with no-flux boundary condition, i.e.,

$$-\Delta \phi_n = \lambda_n \phi_n, \quad \partial_{\mathbf{n}} \phi_n \big|_{\partial \Omega} = 0, \quad \langle \phi_n, \phi_n \rangle = 1. \tag{17}$$

When $\Omega = \{y|y \in [0,1]\}$, we have $\phi_0 = 1$, $\lambda_0 = 0$ and $\phi_n = \sqrt{2}\cos n\pi y$, $\lambda_n = n^2\pi^2$, $n \geq 1$.

Substituting $T = \bar{T} + \theta_1\partial_x\bar{T}$ into the evolution equation of $\bar{T}$, we obtain the first order effective equation

$$\partial_t\bar{T} + \mathrm{Pe}\bar{v}\partial_x\bar{T} = a_2\partial_x^2\bar{T}, \quad a_2 = \left(1 - \mathrm{Pe}\overline{v\theta_1}\right). \tag{18}$$

The classical homogenization approach relies on the Fredholm alternative which involves a space-time average. As a result, the effective equation is a constant coefficient equation even for the time-varying flow case [29, 31]. Here, with the center manifold approach, we obtain the effective equation (18) with time-dependent coefficients which could approximate the scalar field better in an earlier stage. Comparing the definition of Aris moments (see [31]) and variance of the cross-sectional average, we have

$$\mathrm{Var}(\bar{T}) = \mathrm{Var}(\bar{T}_I) + 2\int_0^t a_2(s)\mathrm{d}s. \tag{19}$$

For a periodic time-varying flow [65] and a class of random flows [20, 32], we have $\mathrm{Var}(\bar{T}) = 2\kappa_{\mathrm{eff}}t + \mathcal{O}(1)$, where κ_{eff} is the effective diffusivity

$$\kappa_{\mathrm{eff}} = \lim_{t\to\infty}\frac{\mathrm{Var}(\bar{T})}{2t} = \lim_{t\to\infty}\frac{1}{t}\int_0^t a_2(s)\mathrm{d}s. \tag{20}$$

In other words, a_2 can be approximated by its time average at long times.

Based on equation (16), the effective diffusivity induced by the flow $v(\mathbf{y}, t) = \xi(t)u(\mathbf{y})$ is

$$a_2 = \left(1 - \mathrm{Pe}\overline{v\theta_1}\right) = 1 + \mathrm{Pe}^2\sum_{n=1}^{\infty}\langle u, \phi_n\rangle^2\,\xi(t)\int_0^t e^{\lambda_n(s-t)}\xi(s)\mathrm{d}s,$$

$$\kappa_{\mathrm{eff}} = 1 + \mathrm{Pe}^2\lim_{t\to\infty}\frac{1}{t}\int_0^t\sum_{n=1}^{\infty}\langle u, \phi_n\rangle^2\,\xi(s_2)\int_0^{s_2} e^{\lambda_n(s_1-s_2)}\xi(s_1)\mathrm{d}s_1\mathrm{d}s_2. \tag{21}$$

With the initial condition $T(x, \mathbf{y}, 0) = \left(\sqrt{2\pi}\sigma\right)^{-1}\exp\left(-\frac{x^2}{2\sigma^2}\right)$, the solution of equation (18) gives an approximation of $\bar{T}$ as $t \to \infty$,

$$\bar{T}(x, t) = \frac{1}{\sqrt{2\pi b_2}}\exp\left(\frac{-\tilde{x}^2}{2b_2}\right) + \mathcal{O}(t^{-\frac{3}{2}}),$$

$$b_2(t) = \sigma^2 + 2\int_0^t a_2(s)\mathrm{d}s, \quad \tilde{x} = x - \mathrm{Pe}\int_0^t \bar{v}(s)\mathrm{d}s. \tag{22}$$

For steady flow, we have $b_2 = \sigma^2 + 2\kappa_{\mathrm{eff}}t$. Then equation (22) reduces to the classical Gaussian approximation [26]. Since the scalar field will be homogenized across the channel at long times, $\bar{T}$ itself could be an approximation of T. In fact, we could obtain a more accurate approximation of T,

$$T \approx \bar{T} + \theta_1\partial_x\bar{T} = \left(1 - \frac{\theta_1(\mathbf{y}, t)\tilde{x}}{b_2}\right)\frac{1}{\sqrt{2\pi b_2}}\exp\left(\frac{-\tilde{x}^2}{2b_2}\right) + \mathcal{O}(t^{-\frac{3}{2}}). \tag{23}$$

Since $\partial_x\bar{T}$ is an odd function with respect to x, the error of approximation (23) is still $\mathcal{O}(t^{-\frac{3}{2}})$. However, equation (23) practically performs better than $\bar{T}$ because it depicts the across channel variation of the scalar. To demonstrate that, we numerically solved equation (3) with Pe = 200, $u(y, t) = (\cos\omega t)y(1-y)/2$, and initial condition $T_I = \left(\sqrt{2\pi}\sigma\right)^{-1}\exp\left(-\frac{x^2}{2\sigma^2}\right)$, $\sigma = 1/40$ by the method described in appendix 7.1. Figure 2 presents the relative errors of different approximations, $\|T - T_{approx}\|_{\infty}/\|T\|_{\infty}$. As shown in figure 2, the relative error of approximation (22) (red curve) is around 0.1 at $t = 1$, while, the relative error of approximation (23) (blue curve) is around 10^{-3}. Since two approximations are of the same asymptotic order at long times, presumably the differences between the two approximations will reduce as time is further increased.
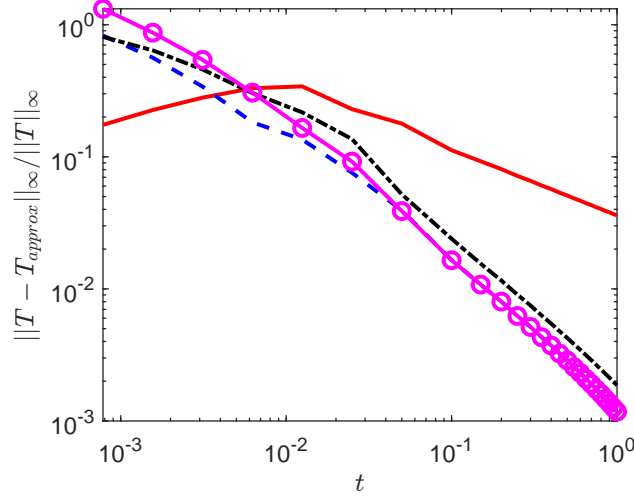
FIG. 2: The relative error of various approximations $\|T - T_{approx}\|_\infty / \|T\|_\infty$ where T is evaluated numerically. The red solid curve, blue dashed curve, black dot-dash curve and purple curve are the relative error of approximation (22), (23), (24) and (25), respectively.

In many applications, the scalar field usually stands for the concentration which must be nonnegative for all times. However, this approximation (23) could be negative for some x and t, which may not be desirable in those applications. [72, 73] proposed the following nonnegative approximation to study the transverse distribution of concentration distribution for the laminar tube flow,

$$T \approx \frac{1}{\sqrt{2\pi b_2}} \exp\left(\frac{-(\tilde{x} - \theta_1(\mathbf{y}, t))^2}{2b_2}\right). \tag{24}$$

The approximation (24) converges asymptotically to approximation (23) as $\theta \to 0$. However, the relative difference between them doesn't vanish as $t \to \infty$. As shown in figure 2, there is a visible difference between the approximation (24) (black curve) and (23) (blue curve).

Here, we propose a different nonnegative asymptotic expansion

$$T \approx \left(1 - \frac{\theta_1(\mathbf{y}, t)\tilde{x}}{2b_2}\right)^2 \frac{1}{\sqrt{2\pi b_2}} \exp\left(\frac{-\tilde{x}^2}{2b_2}\right), \quad t \to \infty. \tag{25}$$

Since the difference between equation (23) and (25) is $\mathcal{O}(t^{-\frac{5}{2}})$, the relative difference between them vanishes as $t \to \infty$. From figure 2, we can see that the relative error of approximation (23) and (25) is almost indistinguishable after $t = 0.1$. We remark that the approximation (25) may not conserve the mass of the scalar at the earlier stage of the evolution. However, the size of the non-conserved mass decays as $\mathcal{O}(t^{-2})$ at long time which is smaller than the error in scalar field in this approximation: $\mathcal{O}(t^{-1})$. Hence, it is a reasonable approximation at long time.

Next, we study the second order approximation of the scalar field. We have to solve the equation for θ_2,

$$(\partial_t - \Delta_\mathbf{y})\theta_2 = -\text{Pe}(v\theta_1 - \theta_1\bar{v} - \overline{v\theta_1}), \quad \left.\frac{\partial}{\partial \mathbf{n}}\theta_2\right|_{\partial\Omega} = 0. \tag{26}$$

We have the expansion of $v\theta_1 - \theta_1\bar{v} - \overline{v\theta_1}$,

$$v\theta_1 - \theta_1\bar{v} - \overline{v\theta_1} = \sum_{n_2, n_1=1}^{\infty} \langle\theta_1, \phi_{n_1}\rangle \langle\phi_{n_1}(v - \bar{v}), \phi_{n_2}\rangle \phi_{n_2}. \tag{27}$$

That leads to the solution

$$\theta_2 = \text{Pe}^2 \sum_{n_2, n_1=1}^{\infty} \langle u, \phi_{n_1}\rangle \langle\phi_{n_1}(u - \bar{u}), \phi_{n_2}\rangle \phi_{n_2} \int_0^t \left(e^{\lambda_{n_2}(s_2-t)}\xi(s_2) \int_0^{s_2} e^{\lambda_{n_1}(s_1-s_2)}\xi(s_1)ds_1\right) ds_2. \tag{28}$$

Substituting $T = \bar{T} + \theta_1 \partial_x \bar{T} + \theta_2 \partial_x^2 \bar{T}$ into the evolution equation of $\bar{T}$, the approximated evolution equation for $\bar{T}$ becomes a linearized Burgers-Korteweg-de Vries equation

$$\partial_t \bar{T} + \bar{v} \partial_x \bar{T} = a_2 \partial_x^2 \bar{T} - a_3 \partial_x^3 \bar{T}, \quad a_3 = \mathrm{Pe}\overline{v\theta_2}. \tag{29}$$

Next we can consider two cases based on $a_3 = \mathrm{Pe}\overline{v\theta_2}$. First, we consider the case $a_3 = \mathrm{Pe}\overline{v\theta_2} = 0$, which implies the skewness of $\bar{T}$ is zero. One such example is the linear shear flow created by moving one boundary of a parallel-plate channel [31]. In this case, the evolution equation for $\bar{T}$ reduces to a diffusion equation, where the Gaussian approximation (22) is still valid. Then we obtain the approximation of the whole scalar field

$$\begin{aligned}
T &= \bar{T} + \theta_1 \partial_x \bar{T} + \theta_2 \partial_x^2 \bar{T} \\
&= \left(1 - \frac{\theta_1 \tilde{x}}{b_2} + \frac{\theta_2 \left(\tilde{x}^2 - b_2 \right)}{b_2^2} \right) \frac{1}{\sqrt{2\pi b_2}} \exp \left(\frac{-\tilde{x}^2}{2b_2} \right) + \mathcal{O}(t^{-2}).
\end{aligned} \tag{30}$$

Since $\partial_x^2 \bar{T}$ is an even function with respect to x, the error of approximation (30) is $\mathcal{O}(t^{-2})$ which is more accurate than the approximation (23).

To demonstrate the validity of the approximation (30), we compare it with the numerical solution of equation (3) with the flow $v(y,t) = \cos \pi y$. The steady solution of equation (15) and (26) are

$$\theta_1 = -\mathrm{Pe}\frac{\cos \pi y}{\pi^2}, \quad \theta_2 = \frac{\mathrm{Pe}^2 \cos(2\pi y)}{8\pi^4}, \quad b_2 = \sigma^2 + \left(\frac{\mathrm{Pe}^2}{\pi^2} + 2 \right) t. \tag{31}$$

To fit the initial condition T_I and increase the accuracy, we can impose the initial condition $\theta_1(y,0) = \theta_2(y,0) = 0$ and obtain the time-dependent solutions,

$$\begin{aligned}
\theta_1 &= -\mathrm{Pe}\frac{\cos \pi y}{\pi^2} \left(1 - e^{-\pi^2 t} \right), \quad \theta_2 = \frac{\mathrm{Pe}^2 \cos(2\pi y)}{8\pi^4} \left(1 - e^{-4\pi^2 t} \right), \\
b_2 &= \sigma^2 + \left(\frac{\mathrm{Pe}^2}{\pi^2} \left(1 - e^{-\pi^2 t} \right) + 2 \right) t.
\end{aligned} \tag{32}$$

Figure 3 shows the relative error of different approximations. The numerical solution is obtained via the method described in detail in appendix 7.1. We have three observations. First, the formula (23) and (30) retaining cross-sectional variation provide more accurate approximation than (22). Second, we can see that the second-order approximation (30) has smaller error than the first-order approximation (23) at larger time. We expect this difference will be more pronounced at longer times. Third, if we impose the initial condition on θ_1 and θ_2, then we obtain a more accurate approximation at an earlier stage.

Next, we consider the case $a_3 \neq 0$. When the initial condition is $T_I(x, \mathbf{y}) = \delta(x)$, the integral representation of the solution is

$$\bar{T}(x,t) = \frac{1}{2\pi} \int_{-\infty}^{\infty} e^{-\frac{1}{2}b_2 k^2 - ik^3 \int_0^t a_3(s)\mathrm{d}s + ixk} \, \mathrm{d}k = \frac{1}{\pi} \int_0^{\infty} e^{-\frac{1}{2}b_2 k^2} \cos \left(-k^3 \int_0^t a_3(s)\mathrm{d}s + xk \right) \mathrm{d}k. \tag{33}$$

We are interested in the asymptotic expansion of solution (33) at long times. It is a hard task for a general time-varying flow. Therefore, we restrict our attention to the case where a_2, a_3 are constant. For some time-varying flows, we can approximate a_2, a_3 with their time average at long times, for example, periodic time-varying flow. Hence, the asymptotic expansion we derived in the section also applies to these cases.

If $x \ll t$ and $t \to \infty$, the integrand in equation (33) is localized around $k = 0$. Hence, we have the approximation

$$\begin{aligned}
\bar{T}(x,t) &= \int_{-\infty}^{\infty} \left(1 - ia_3 k^3 t + \frac{(-ia_3 k^3 t)^2}{2} \right) \exp(-a_2 k^2 t + ixk) + \mathcal{O}(t^{-2}) \\
&= \left(1 - \frac{a_3}{2^3 a_2^{\frac{3}{2}} t^{\frac{1}{2}}} H_3 \left(\frac{x}{2\sqrt{a_2 t}} \right) + \frac{a_3^2}{2^7 a_2^3 t} H_6 \left(\frac{x}{2\sqrt{a_2 t}} \right) \right) \frac{\exp \left(\frac{-x^2}{4a_2 t} \right)}{\sqrt{4\pi a_2 t}} + \mathcal{O}(t^{-2}),
\end{aligned} \tag{34}$$

where H_n is the degree n Hermite polynomial associated with the weight function e^{-x^2}. The approximation (34) is identical to the Hermite polynomial representation proposed in equation (5.7) in [59].
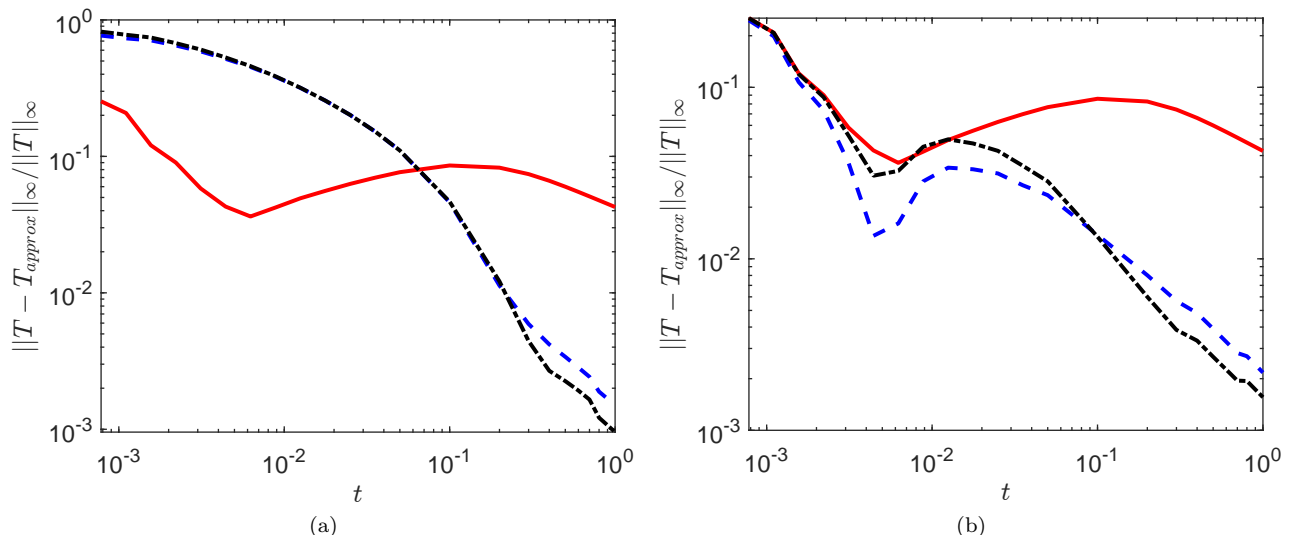
FIG. 3: The relative error of various approximations of numerical solution of equation (3) with the flow $v(y,t) = \cos \pi y$, Pe $= 1$ and initial condition $T_I = \left(\sqrt{2\pi}\sigma\right)^{-1} \exp\left(-\frac{x^2}{2\sigma^2}\right), \sigma = 1/20$. The red solid, blue dashed and black dot-dash curve represent the relative error of approximation (22), (23) and (30). Panel (a) θ_1 and θ_2 are provided in equation (31). Panel (b) θ_1 and θ_2 are provided in equation (32)

Last, we remark that for the initial condition discussed in this section, b_2 and $\int_0^t a_3(s)\mathrm{d}s$ are related to the variance and skewness provided in equation (4) and (5) respectively. For the general time-varying flows, the eigenfunction series expansions of variance and skewness are valid in [31, 65, 66]. Additionally, we would refer to table 1 in [29] which presents a summary of flows and the methodologies used in the prior literature.

3.3. Improvements compared with previous studies

We remark that there are two subtle differences compared with the previous studies [45, 48, 49]. First, the previous studies made not only the ansatz of the expansion of T, but also the expansion of $\bar{T}$. Therefore, the recursive equations involve not only θ_n, but also the coefficients in the expansion of $\bar{T}$. Here, we avoid making the expansion ansatz for $\bar{T}$ by utilizing equation (12a), which simplifies the calculation of θ_n.

Second, in the previous studies, time is considered as a parameter rather than a dependent variable of the system. Hence, the equation for the auxiliary function θ_1 derived in [45, 48, 49] takes the form

$$-\Delta_{\mathbf{y}}\theta_1 = -\mathrm{Pe}(u - \bar{u}), \tag{35}$$

in which the time derivative term doesn't appear. One possible justification for this approximation could be that the flow $u(\mathbf{y}, t)$ varies slowly in time so that the time derivative term is negligible. However, in situations involving flows admitting rapid temporal evolution, this approximation will be invalid. Let's consider a simple example, $\Omega = [0, 1]$, Pe $= 1$, $u = -e^{\mathrm{i}\omega t} \cos \pi y$. The solution of equation (15) is $\frac{e^{\mathrm{i}\omega t} \cos \pi y}{\pi^2 + \mathrm{i}\omega}$, while the solution of equation (35) is $\frac{e^{\mathrm{i}\omega t} \cos \pi y}{\pi^2}$. The only difference between them is the denominator, which yields a $\mathcal{O}(\omega)$ difference. Hence, for $\omega \ll 1$, the two solutions are close. However, for any fixed ω, the corresponding approximations of the solute distribution T diverge at long times, due to the variances having different growth rates. Recall that the variance,$\mathrm{Var}(\bar{T}) = 2(1 - \mathrm{Pe}\overline{v\theta_1})t + \mathcal{O}(1)$, grows linearly at long times. The difference between the two variances arising from the two different cell problems accumulates and becomes an $\mathcal{O}(1)$ difference at the frequency time scale $\mathcal{O}\left(\omega^{-1}\right)$. Since the solute distribution is characterized by the variance, the $\mathcal{O}(1)$ difference between variances implies an $\mathcal{O}(1)$ difference in the distributions at that time. Moreover, this difference in distributions will keep increasing as time increases. Hence, we conclude that equation (35) should only be used with a slow varying flow and before the frequency time scale. In addition, this can be considered an example of non-commutating limits.

We know the center manifold becomes a good approximation if the exponential correction is small, i.e., after the diffusion time scale L^2/κ, which is independent of the frequency time scale of the flow. However, the simplification in

equation (35) makes the approximation unlikely to be valid after the frequency time scale. Hence, if the frequency time scale is less than the diffusion time scale, then equation (35) is invalid for all time. That certainly limits the application of the result based on equation (35). [45, 46] adopted equation (35) to study dispersion induced by pulsating flows. One of their applications is blood flow. Consider the following practical example. The typical frequency time scale in the human blood vessel is 1s (60 heartbeats per min). The sodium chloride ($\kappa \approx 1.6 * 10^{-5} cm^2/s$ in water [37]) diffuses cross the blood vessel with diameter 0.2 mm takes around 25 s. In this case, the result based on (35) is unlikely valid.

To demonstrate the validity of our analysis, we solve equation (3) numerically and present the results in figure 4. For the time varying shear flow $u(y) = \xi(t)y(1-y)/2$, [48] derived the effective equation

$$\partial_t \bar{T} + \frac{\mathrm{Pe}\xi(t)}{12}\partial_x \bar{T} = \left(1 + \frac{\mathrm{Pe}^2\xi(t)^2}{30240}\right)\partial_x^2\bar{T}. \tag{36}$$

If $\xi(t) = \cos\omega t$, the solution of equation (15) is

$$\theta = \mathrm{Pe}\sum_{n=1}^{\infty}\frac{(-1)^n + 1}{\pi^2 n^2}\cos n\pi y\left(\frac{\omega\sin(t\omega)}{\pi^4 n^4 + \omega^2} + \frac{\pi^2 n^2\cos(t\omega)}{\pi^4 n^4 + \omega^2} - \frac{\pi^2 n^2\mathrm{Pe}e^{-\pi^2 n^2 t}}{\pi^4 n^4 + \omega^2}\right). \tag{37}$$

Hence the effective equation (18) derived by time-dependent center manifold theory is

$$\partial_t\bar{T} + \frac{\mathrm{Pe}\cos\omega t}{12}\partial_x\bar{T} = \left(1 + \mathrm{Pe}^2\sum_{n\in\mathrm{even}^+}^{\infty}\frac{2\cos^2(t\omega)}{\pi^2 n^2\left(\pi^4 n^4 + \omega^2\right)} + \frac{\omega\sin(2t\omega)}{\pi^4 n^4\left(\pi^4 n^4 + \omega^2\right)}\right)\partial_x^2\bar{T}, \tag{38}$$

where we neglect the exponential term in the solution of equation (15). When $t \gg \omega^{-1}$, we could approximate the series in the effective equation by its time average

$$\partial_t\bar{T} + \frac{\mathrm{Pe}\cos\omega t}{12}\partial_x\bar{T} = \left(1 + \mathrm{Pe}^2\left(\frac{1}{24\omega^2} - \frac{\sin\left(\frac{\sqrt{\omega}}{\sqrt{2}}\right) - \sinh\left(\frac{\sqrt{\omega}}{\sqrt{2}}\right)}{4\sqrt{2}\omega^{5/2}\left(\cos\left(\frac{\sqrt{\omega}}{\sqrt{2}}\right) - \cosh\left(\frac{\sqrt{\omega}}{\sqrt{2}}\right)\right)}\right)\right)\partial_x^2\bar{T}. \tag{39}$$

which is identical to the result of standard homogenization theory [29, 31]. Equation (39) is simpler and performs as well as equation (38) at sufficiently large time scales. Of course, at intermediate times scales or in the case with irregular fluctuating flows, equation (38) performs better.

Figure 4 shows the comparison of the numerical solution and different approximations at diffusion time scale $t = 1$. The left column shows the result for a small frequency, $\omega = \pi/5$. The cross-sectional average of the numerical solution, the solution of effective equations (36) and (38) are almost indistinguishable. Recall that the standard homogenization result (39) requires $t \gg \mathcal{O}(\frac{1}{\omega})$. As we expected, the standard homogenization result on this timescale is substantially worse than both center manifold results. Alternatively, at higher frequency, with $\omega = 20\pi$, (36) performs visibly worse than both standard homogenization (39) as well as the time-dependent center manifold results (38). These observations from the numerical simulation are consistent with our previous theoretical analysis.

4.   TIME VARYING RANDOM FLOWS

Most studies of Taylor dispersion focused on periodic time varying flows, fewer studies have addressed irregularly fluctuating flows and even random flows. In this section, we will show that the theory we developed in the previous section can be applied to time varying random flows. Moreover, for random flows involving a white noise process or renewing processes, we show that the effective diffusivity is deterministic at long times. This is also inspired by our work [32] which studied the advection-diffusion equation with the shear flow $(v(y, \xi(t)), 0)$ where $\xi(t)$ is a stationary Ornstein-Uhlenbeck (OU) process in parallel-plate channels enforcing the no-flux boundary conditions. In that work, we derived the effective equation at long times via analyzing the N-point correlation function of the random scalar field. The analysis shows an interesting result that, in this random system, the effective diffusivity is deterministic at long times. We mention an interesting study regarding the ensemble average for a different system without physical boundary conditions. In [53] the authors considered a diffusing passive scalar advected by a non-sheared, two-dimensional sinusoidal flow with a random phase shift in an unbounded domain using an operator splitting method (applying the advection operator and diffusion operator successively). They demonstrated that a
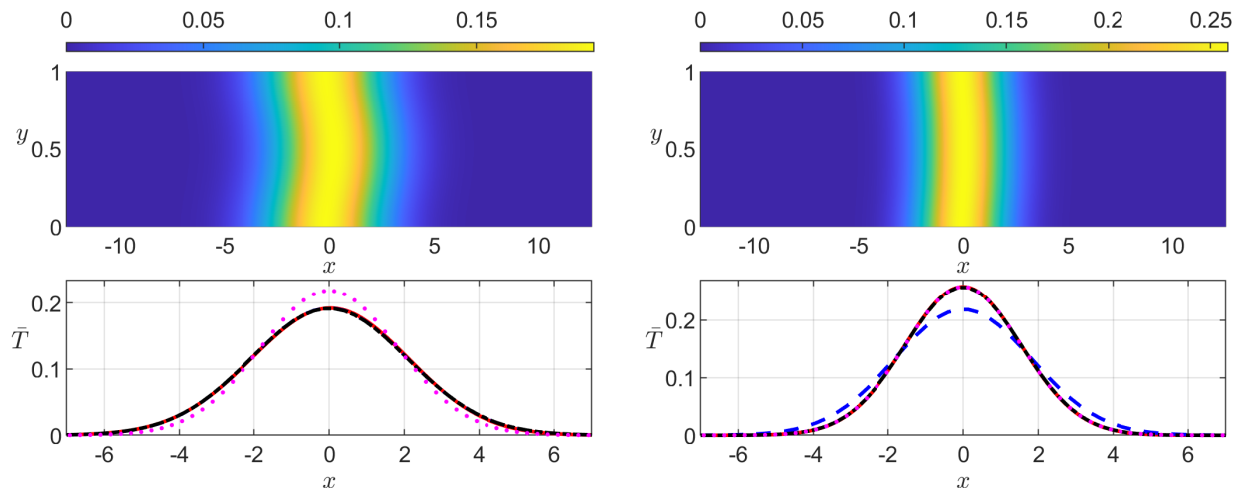
FIG. 4: The first row shows the numerical solution of equation (3) at $t = 1$ with the shear flow $u(y,t) = (\cos \omega t)\, y(1-y)/2$, Pe $= 200$ and initial condition $T_I = \left(\sqrt{2\pi}\sigma\right)^{-1} \exp\left(-\frac{x^2}{2\sigma^2}\right), \sigma = 1/40$, where $\omega = \pi/5$ in left panel, and $\omega = 20\pi$ in right column. In the second row, the red curve is the cross sectional average of the numerical solution. The blue dash curve is the solution of equation (36). The black dot-dash curve is the solution of equation (38). The purple dot curve is the solution of equation (39).

single-realization and ensemble-average effective diffusivities are the same and applied the conclusions to the Fisher-Kolmogorov-Petrovskii-Piskunov (FKPP) model.

We study two cases of flow in this paper. The first case we considered is a Gaussian white noise process $\xi(t)$ which is a zero-mean, Gaussian random process whose correlation function is given by $\langle \xi(t)\xi(s)\rangle = \delta(t - s)$. The center manifold approach is valid for a smoothly varying velocity field. As for the Gaussian white noise which is non-differentiable, we can consider a sequence of functions that converges to the white noise process. The Wong-Zakai theorem states [33, 38, 71] that the convergence of a process to white noise process yields the convergence of the systems driven by them. That justifies the application of the center manifold approach in the non-differentiable case involving white noise. Additionally, [67] showed how to apply the stochastic center manifold theory rigorously to analyze a one dimensional reaction-diffusion equation with white noise terms.

Since the white noise process has a zero correlation time, we can approximate the time dependent diffusion coefficient a_2 with its time average at the diffusion time scale, namely the effective diffusivity κ_{eff}. By utilizing the ergodicity of the white noise process, or equivalently considering the Riemann sum and the law of large number, we have $\lim_{t\to\infty} \frac{1}{t} \int_0^t \xi(s_2) \int_0^{s_2} e^{\lambda_n(s_1 - s_2)} \xi(s_1) \mathrm{d}s_1 \mathrm{d}s_2 = 1$ for all integer $n \geq 1$. Equation (21) reduces to,

$$\kappa_{\text{eff}} = 1 + \text{Pe}^2 \sum_{n=1}^{\infty} \langle u, \phi_n \rangle^2 = 1 + \text{Pe}^2 \left(\frac{1}{|\Omega|} \int_{\Omega} u^2(\mathbf{y}) \mathrm{d}\mathbf{y} - \left(\frac{1}{|\Omega|} \int_{\Omega} u(\mathbf{y}) \mathrm{d}\mathbf{y} \right)^2 \right). \tag{40}$$

Equation (40) is identical to equation (18) in [32] which is derived via the rigorous analysis of N-point correlation function and Hausdorff moment problem. For the system with the random flows, in general, one has to repeat the experiment with different realizations of the flows to obtain the properties of the passive scalar via ensemble average. However, the deterministic diffusivity presented in equation (40) implies that one need only observe a *single* realization of the passive scalar to access some measurable quantities.

Second, we switch our attention to a class of stochastic flows with a finite correlation time. Consider a shear flow takes the form $(A(t)\xi(t)u(\mathbf{y}), 0)$, where $\xi(t)$ is periodic function with a base frequency ω, or equivalent, a period $L_t = \frac{2\pi}{\omega}$. $A(t)$ is a piecewise-constant zero-mean random function of time,

$$A(t) = A_n, \quad nL_t \leq t < (n+1)L_t, \quad n \in \mathbb{Z}, \tag{41}$$

where A_n is an independent and identically distributed random variable with zero mean and finite variance. This type of flow is in the class of renewing (renovating, innovation) flows, that is, flows that decorrelate completely in
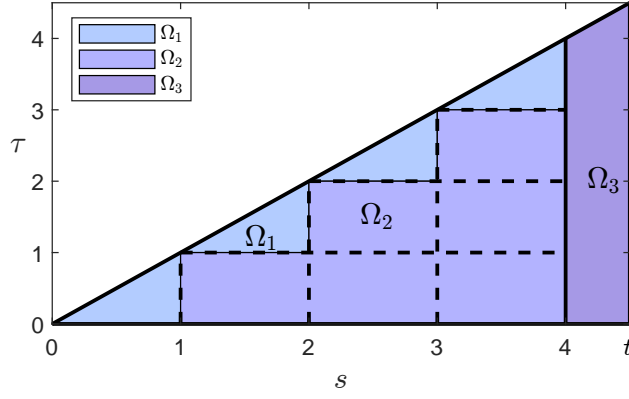
FIG. 5: A schematic of domain tessellation. Ω_i, $i = 1, 2, 3$ are defined in equation (43). The parameters are $t = 4.5$, $L_t = 1$.

a finite time, taken here to be the period L_t. Therefore, although it is not a stationary and ergodic process, it is a good approximation to a stationary process with a finite correlation time. It has wide applications in the study of the dynamo [14, 75] as well as in study of the intermittency of passive-scalar decay[1, 39, 64]. For this type of flow, the closed evolution equation for the statistical moment is unknown. Hence, the Hausdorff moment problem approach proposed in [32] for rigorously studying the white noise flow case doesn't apply to this case. However, we could apply the center manifold approach to near rigorously derive the effective equation at long times.

In this case, the time averaged diffusion coefficient is

$$\kappa_{\text{eff}} = 1 + \lim_{t \to \infty} \frac{\text{Pe}^2}{t} \sum_{n=1}^{\infty} \langle u, \phi_n \rangle^2 \int_0^t \int_0^s e^{-\lambda_n(s-\tau)} \xi(s) A(s) \xi(\tau) A(\tau) \mathrm{d}\tau \mathrm{d}s. \tag{42}$$

We can further simplify this formula by taking advantage of the periodicity. As presented in figure 5, we tessellate the integral domain by squares and divided the domain into three regions,

$$\begin{aligned}
\Omega_1 &= \bigcup_{k=0}^{\lfloor \frac{t}{L_t} \rfloor - 1} \left\{ (s, \tau) | s \in [kL_t, (k+1)L_t], \tau \in [kL_t, s] \right\}, \\
\Omega_2 &= \bigcup_{k=0}^{\lfloor \frac{t}{L_t} \rfloor - 1} \left\{ (s, \tau) | s \in [kL_t, (k+1)L_t], \tau \in [0, kL_t] \right\}, \\
\Omega_3 &= \left\{ (s, \tau) | t \in [L_t \lfloor \frac{t}{L_t} \rfloor, t], \tau \in [0, s] \right\}.
\end{aligned} \tag{43}$$

According to this integral domain partition, we divide the double integral in equation (42) into three parts,

$$\begin{aligned}
\iint_{\Omega_1} \ldots \mathrm{d}\tau \mathrm{d}s &= \sum_{m_1=0}^{\lfloor \frac{t}{L_t} \rfloor - 1} A_{m_1}^2 \int_{m_1 L_t}^{(m_1+1)L_t} \int_{m_1 L_t}^s e^{-\lambda_n(s-\tau)} \xi(s) \xi(\tau) \mathrm{d}\tau \mathrm{d}s, \\
\iint_{\Omega_2} \ldots \mathrm{d}\tau \mathrm{d}s &= \sum_{m_1=1}^{\lfloor \frac{t}{L_t} \rfloor - 1} \sum_{m_2=0}^{m_1} A_{m_1} A_{m_2} \int_{m_1 L_t}^{(m_1+1)L_t} \int_{m_2 L_t}^{(m_2+1)L_t} e^{-\lambda_n(s-\tau)} \xi(s) \xi(\tau) \mathrm{d}\tau \mathrm{d}s, \\
\iint_{\Omega_3} \ldots \mathrm{d}\tau \mathrm{d}s &= A_{\lfloor \frac{t}{L_t} \rfloor} \int_{L_t \lfloor \frac{t}{L_t} \rfloor}^t \int_0^s e^{-\lambda_n(s-\tau)} \xi(s) A(\tau) \xi(\tau) \mathrm{d}\tau \mathrm{d}s,
\end{aligned} \tag{44}$$

where we omit the lengthy integrand on the left hand side of equations. In fact, only the integral over Ω_1 grows linearly on time and contributes to the effective diffusivity. With rearranging the order of the double summation, the

integral over Ω_2 becomes

$$\sum_{m_1=1}^{\lfloor\frac{t\omega}{2\pi}\rfloor-1}\sum_{m_2=0}^{m_1}A_{m_1}A_{m_2}e^{-\lambda_n\frac{2\pi(m_1-m_2)}{\omega}}\int_0^{\frac{2\pi}{\omega}}\int_0^{\frac{2\pi}{\omega}}e^{-\lambda_n(s-\tau)}\xi(s)\xi(\tau)\mathrm{d}\tau\mathrm{d}s$$

$$=\sum_{q=1}^{\lfloor\frac{t\omega}{2\pi}\rfloor-1}\left(e^{-\lambda_n\frac{2\pi q}{\omega}}\sum_{m_1=q}^{\lfloor\frac{t\omega}{2\pi}\rfloor-1}A_{m_1}A_{m_1-q}\right)\int_0^{\frac{2\pi}{\omega}}\int_0^{\frac{2\pi}{\omega}}e^{-\lambda_n(s-\tau)}\xi(s)\xi(\tau)\mathrm{d}\tau\mathrm{d}s \tag{45}$$

$$=\int_0^{\frac{2\pi}{\omega}}\int_0^{\frac{2\pi}{\omega}}e^{-\lambda_n(s-\tau)}\xi(s)\xi(\tau)\mathrm{d}\tau\mathrm{d}s\sum_{q=1}^{\lfloor\frac{t\omega}{2\pi}\rfloor-1}e^{-\lambda_n\frac{2\pi q}{\omega}}o(\lfloor\frac{t\omega}{2\pi}-1-q\rfloor)=o\left(\lfloor\frac{t\omega}{2\pi}\rfloor\right),$$

where the last line follows the law of large numbers, namely $\frac{1}{\lfloor\frac{t\omega}{2\pi}\rfloor-1-q}\sum_{m_1=q}^{\lfloor\frac{t\omega}{2\pi}\rfloor-1}A_{m_1}A_{m_1-q}=E(A_qA_0)+o(1)$ almost surely for a fixed q. Then the whole integral vanishes after dividing by t and taking the long time limit.

Next, the integral over Ω_3 in equation (44) is an integral over a bounded interval $s\in[L_t\lfloor\frac{t}{L_t}\rfloor,t]$. It is enough to show the integrand is a bounded function of s on this interval. We have

$$\int_0^s e^{-\lambda_n(s-\tau)}\xi(s)A(\tau)\xi(\tau)\mathrm{d}\tau$$

$$=A_{\lfloor\frac{t\omega}{2\pi}\rfloor}\int_{\frac{2\pi}{\omega}\lfloor\frac{t\omega}{2\pi}\rfloor}^s e^{-\lambda_n(s-\tau)}\xi(s)\xi(\tau)\mathrm{d}\tau+\sum_{m_2=0}^{\lfloor\frac{t\omega}{2\pi}\rfloor-1}A_{m_2}\int_{\frac{2\pi m_2}{\omega}}^{\frac{2\pi(m_2+1)}{\omega}}e^{-\lambda_n(s-\tau)}\xi(s)\xi(\tau)\mathrm{d}\tau \tag{46}$$

$$=A_{\lfloor\frac{t\omega}{2\pi}\rfloor}\int_{\frac{2\pi}{\omega}\lfloor\frac{t\omega}{2\pi}\rfloor}^s e^{-\lambda_n(s-\tau)}\xi(s)\xi(\tau)\mathrm{d}\tau+\sum_{m_2=0}^{\lfloor\frac{t\omega}{2\pi}\rfloor-1}A_{m_2}e^{-\lambda_n\left(s-\frac{2\pi m_2}{\omega}\right)}\int_0^{\frac{2\pi}{\omega}}e^{\lambda_n\tau}\xi(s)\xi(\tau)\mathrm{d}\tau,$$

where both terms in the last step are bounded functions of s.

Hence, the integral over Ω_2 and Ω_3 in equation (44) vanishes after dividing by t and taking the long time limit. Now, we have the leading order approximation of equation (42) at long times,

$$\kappa_{\mathrm{eff}}=1+\lim_{t\to\infty}\frac{\mathrm{Pe}^2}{t}\sum_{n=1}^\infty\langle u,\phi_n\rangle^2\int_0^{\frac{2\pi}{\omega}}\int_0^s e^{-\lambda_n(s-\tau)}\xi(s)\xi(\tau)\mathrm{d}\tau\mathrm{d}s\sum_{m_1=0}^{\lfloor\frac{t\omega}{2\pi}\rfloor-1}A_{m_1}^2+\mathcal{O}(t^{-1})$$

$$\tag{47}$$

$$=1+\frac{\mathrm{Pe}^2\omega}{2\pi}\mathrm{Var}(A_0)\sum_{n=1}^\infty\langle u,\phi_n\rangle^2\int_0^{\frac{2\pi}{\omega}}\int_0^s e^{-\lambda_n(s-\tau)}\xi(s)\xi(\tau)\mathrm{d}\tau\mathrm{d}s.$$

where the second step follows the law of large numbers.

It is natural to compare the renewing flow $(A(t)\xi(t)u(\mathbf{y}),\mathbf{0})$ with its deterministic counterpart $(\mathrm{var}(A_0)\xi(t)u(\mathbf{y}),\mathbf{0})$, and ask the question which one induces a larger effective diffusivity. One may expect the random motion creates a larger dispersion. However, it is not always true. A counter example is the $\xi(t)=\cos t$, $\mathrm{Pe}=1$ and $\mathrm{Var}(A)=1$, where the effective diffusivity induced by the renewing flow is $\kappa_{\mathrm{eff,r}}\approx1.3993$, while the effective diffusivity induced by its deterministic counterpart is $\kappa_{\mathrm{eff,d}}\approx1.4124$.

Interestingly, if we impose the continuity assumption on the renewing flow, then we have $\kappa_{\mathrm{eff,r}}\geq\kappa_{\mathrm{eff,d}}$. The continuity of $A(t)\xi(t)$ implies $\xi(0)=\xi(L_t)=0$. Hence, $\xi(t)$ admits a sine expansion $\xi(t)=\sum_{k=1}^\infty c_k\sin k\omega t$. Recall that, in the calculation of effective diffusivity induced by the renewing flow, the contribution of the integral over Ω_2 in equation (44) vanishes due to the mean zero property of the random process $A(t)$. However, when $A(t)$ is a deterministic function, this term grows linearly on time and contributes to the effective diffusivity. Therefore, it is

enough to establish that this term is non-positive. We have

$$\int_{m_1 L_t}^{(m_1+1)L_t} \int_{m_2 L_t}^{(m_2+1)L_t} e^{-\lambda_n(s-\tau)}\xi(s)\xi(\tau)\mathrm{d}\tau\mathrm{d}s$$

$$=e^{-\lambda_n L_t(m_1-m_2)} \int_0^{\frac{2\pi}{\omega}} \int_0^{\frac{2\pi}{\omega}} e^{-\lambda_n(s-\tau)}\xi(s)\xi(\tau)\mathrm{d}\tau\mathrm{d}s \qquad (48)$$

$$=e^{-\lambda_n L_t(m_1-m_2)} \sum_{k_1,k_2=1}^{\infty} c_{k_1} c_{k_2} C_{k_1,k_2},$$

where $C_{k_1,k_2} = \int_0^{\frac{2\pi}{\omega}} \int_0^{\frac{2\pi}{\omega}} e^{-\lambda_n(s-\tau)}\sin(k_2\omega s)\sin(k_1\omega\tau)\mathrm{d}\tau\mathrm{d}s$. It is enough to show the (possibly infinite) matrix C is semi-negative definite. In fact, we have

$$C_{k_1,k_2} = -4\omega^2 \sinh^2\left(\frac{\pi^3 n^2}{\omega}\right) \frac{k_1}{k_1^2\omega^2 + \lambda_n^2} \frac{k_2}{k_2^2\omega^2 + \lambda_n^2}. \qquad (49)$$

Hence, for any n, C is a rank one matrix with only one negative eigenvalue, which implies C is semi-negative definite. Now, we finished the proof of $\kappa_{\mathrm{eff,r}} \geq \kappa_{\mathrm{eff,d}}$ for the continuous renewing flow.

To verify our theoretical results regarding the deterministic effective diffusivity, we solve equation (3) with shear flows $v(y,t) = (y-1/2)A(t)\sin 100\pi t$ by using the forward Monte-Carlo method described in [31]. The computational domain is $(x,y) \in \mathbb{R} \times [0,1]$. The time step size is 10^{-3}. The total number of the random walkers is 2×10^6. We divide a simulation into 400 parallel jobs on UNC's Longleaf computing cluster. In panel (a,b,c,d,e), Pe = 400. In panel (f), Pe = 1200. In panel (a), $A(t)$ is a white noise process. In panel (b), $A(t) = 1$. $A(t)$ is a renewing process with a coin-toss random variable taking values plus or minus one with equal probability in panel (c), a standard Gaussian distributed random variable respectively in panel (d) and a uniform distributed random variable on $[-\sqrt{3}, \sqrt{3}]$ in panel (e,f). We plot $\frac{\mathrm{Var}(\bar{T})}{2t}$ as a function of time for 5 independent flow realizations and different shear flows in figure 6. The curves with the same color are generated with the same seed from the same random number generator.

From figure 6, we have five observations. First, in panel (a,c,d,e,f), all curves fluctuate randomly at the earlier stage but converge at later times to a deterministic effective diffusivity κ_{eff} given by equation (47). Second, since all distributions in panel (c, d, e) have the same unit variance, all renewing flows induce the same effective diffusivity at long times. Third, comparing panel (b) and panel (c, d, e), we can see that renewing random flows induce a larger effective diffusivity than their deterministic counterpart, as just proven above. Fourth, from the right column of figure 6, we can see that if the distribution of $A(t)$ has a heavier tail, then $\frac{\mathrm{Var}(\bar{T})}{2t}$ takes a longer time to converge to the theoretical limit. Fifth, the long-time asymptotic correction of effective diffusivity is proportional to the square of the Péclet number. Hence, for a larger Péclet number, it will take a longer time to converge in the sense of the absolute difference. However, notice that the effective diffusivity is also proportional to the square of the Péclet number. We expect it will take a similar time to achieve the same relative difference. Panel (e,f) supports this analysis.

4.1. Invariant measure

Equation (22) is an approximation of the scalar field at long times, which is a powerful tool to compute the invariance measure of the random field. Let's consider the flow we discussed in the previous section. First, when $v(y,t) = \xi(t)u(\mathbf{y})$ and $\xi(t)$ is the Gaussian white noise, equation (22) becomes

$$\bar{T}(x,t) = \frac{1}{\sqrt{4\pi\kappa_{\mathrm{eff}}t}} \exp\left(\frac{-\tilde{x}^2}{4\kappa_{\mathrm{eff}}t}\right) + \mathcal{O}(t^{-\frac{3}{2}}), \quad \tilde{x} = x - \mathrm{Pe}\bar{u}B(t), \qquad (50)$$

where $B(t)$ is the standard Brownian motion and κ_{eff} is provided in (40). Even though the effective diffusivity is deterministic at long time, generally, the scalar itself may still be random at long time, and the availability of the invariant measure is useful. To that end, we apply the inverse transform method (we refer reader to [18] for details) to obtain the invariant measure of $\bar{T}$, i.e, the probability density function at long times, from the probability density
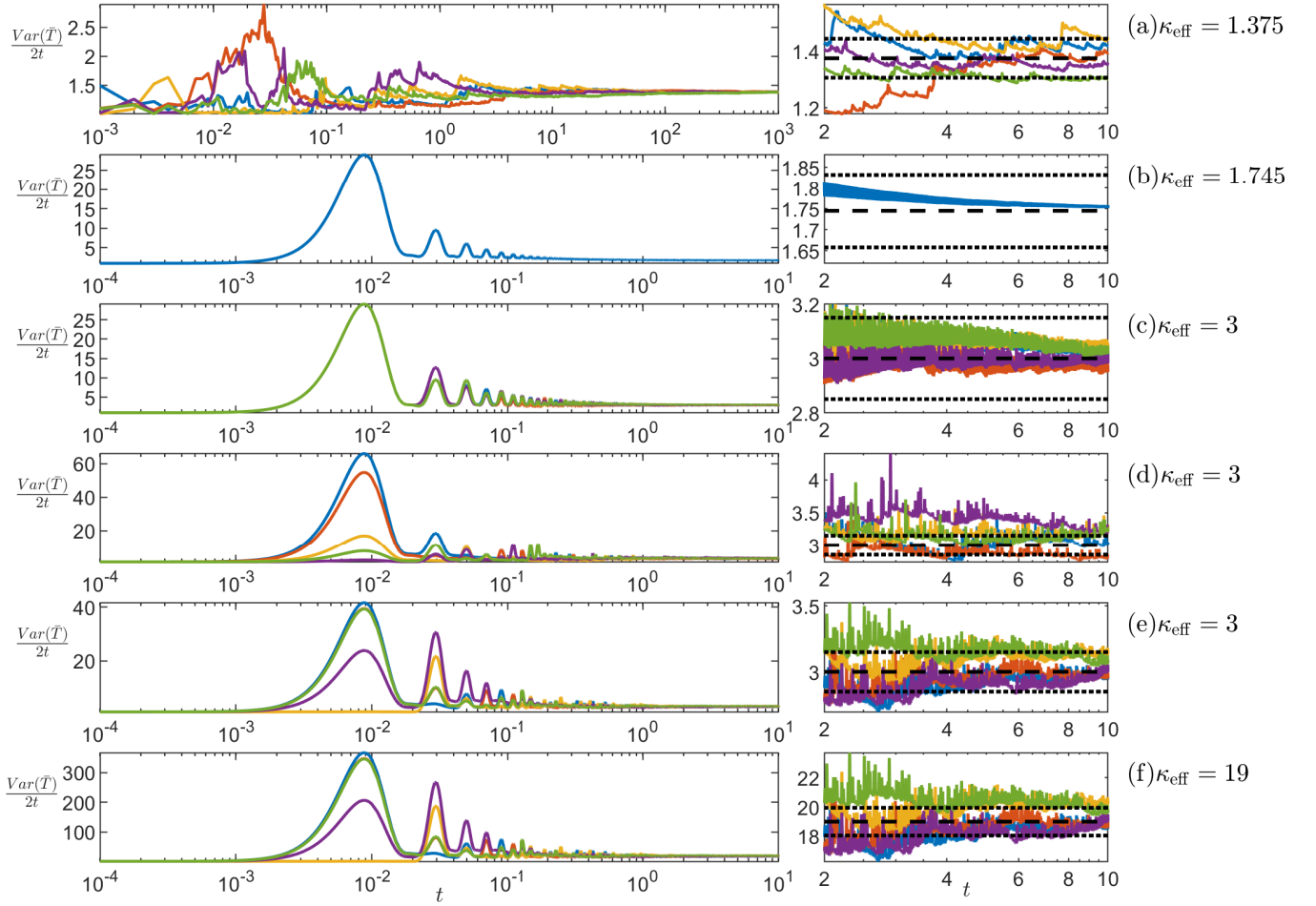
FIG. 6: $\frac{\text{Var}(\bar{T})}{2t}$ as a function of time for 5 independent flow realizations and different random flows. Note that equation (4) shows this quantity converges to the deterministic effective diffusivity at long times. We compute κ_{eff} by equation (40) for panel (a), by equation (21) for panel (b), by equation (47) for panel (c, d, e, f) and report three significant digits of the effective diffusivity to the right of each row. Pictures in the right column are simply zoom-in of pictures in the left column at a larger time scale. The black dashed line indicates the theoretical limit κ_{eff}. The dotted lines are $0.95\kappa_{\text{eff}}$ or $1.05\kappa_{\text{eff}}$.

function of $B(s)$. We consider the rescaling of T, $\tilde{T}(x, y, t) = \sqrt{4\pi\kappa_{\text{eff}}t}T$. Without loss of generality, we focus on the scalar at point $x = 0, y = 0$, i.e., $\tilde{T}(0, 0, t)$. Thus, the invariant measure is

$$f_{\tilde{T}}(z) = \frac{z^{\frac{1}{\beta}-1}}{\sqrt{-\pi\beta\log(z)}}, \quad z \in [0, 1], \tag{51}$$

where $\beta = \frac{\text{Pe}^2\bar{u}^2v(t)}{2t\kappa_{\text{eff}}} = \frac{\text{Pe}^2\bar{u}^2}{2\kappa_{\text{eff}}} + \mathcal{O}(t^{-1})$ and $v(t)$ is the variance of $\int_0^t \xi(s)\mathrm{d}s$. $f_{\tilde{T}}(z)$ always has the logarithmic singularity at $z = 1$. It is continuous at $z = 0$ when $\beta \leq 1$, and singular when $\beta > 1$ (see figure 7). Some physical insight can help interpret this result: Indeed, for a weak input random signal, the scalar flied is nearly deterministic. Hence, the rescaled T at $x = 0$ is thus very likely to be 1. As the strength of the random signal increases, white noise flow makes the blob to be most of the time away from the initial position and the value of scalar at original point is more likely to be zero. As a result of that, when the strength of the input random signal exceeds some certain threshold, the distribution changes from negatively-skewed to positively-skewed as β increases.

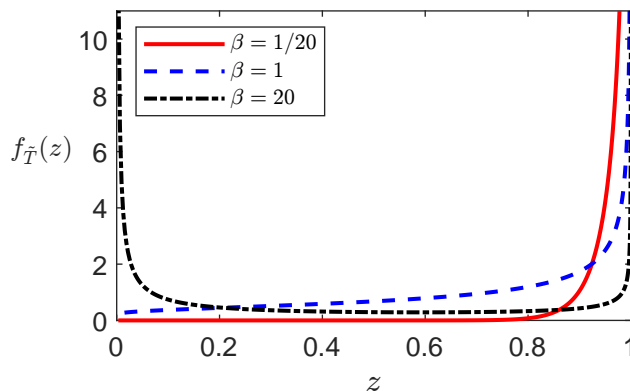Second, when the shear flow is the renewing flow $v(y, t) = A(t)\xi(t)u(y)$, we also have the Gaussian function

FIG. 7: The invariant measure $f_{\tilde{T}}(z)$ in equation (51) for different parameters β. The red solid curve, blue dashed curve and black dot-dash curve stand for the case $\beta = 1/20, 1, 20$, respectively. $f_{\tilde{T}}(z)$ changes from negatively-skewed to positively-skewed as β increases.

approximation (22) with the effective diffusivity provided in equation (47) and

$$
\tilde{x} = x - \text{Pe}\bar{u} \int_0^t A(s)\xi(s)\mathrm{d}s = x - \text{Pe}\bar{u} \left(\sum_{n=0}^{\lfloor \frac{t}{L_t} \rfloor - 1} A_n \int_0^{L_t} \xi(s)\mathrm{d}s + A_{\lfloor \frac{t}{L_t} \rfloor} \int_{L_t \lfloor \frac{t}{L_t} \rfloor}^t \xi(t) \right). \tag{52}
$$

The rescaled scalar $\tilde{T}(x,t)$ becomes

$$
\tilde{T}(x,t) = \sqrt{4\pi\kappa_{\text{eff}}t}\,T = \exp\left(-\frac{\left(\text{Pe}\bar{u}X \int_0^{L_t} \xi(s)\mathrm{d}s \right)^2}{4\kappa_{\text{eff}}L_t} \right) + \mathcal{O}\left(t^{-1} \right), \tag{53}
$$

where $X = \frac{1}{\sqrt{\lfloor \frac{t}{L_t} \rfloor}} \sum_{n=0}^{\lfloor \frac{t}{L_t} \rfloor - 1} A_n \sim \mathcal{N}(0, \text{Var}(A_0))$ as $t \to \infty$ follows the central limit theorem. With the same method, we find that the PDF of $\tilde{T}$ takes the same form provided in equation (51), but with a different expression of parameter $\beta = \frac{\left(\text{Pe}\bar{u} \int_0^{L_t} \xi(s)\mathrm{d}s \right)^2 \text{Var}(A_0)}{2\kappa_{\text{eff}}L_t}$. Hence, the renewing flows induces a same type of invariant measure as the one induced by the white noise process at long times.

When $\int_0^{L_t} \xi(s)\mathrm{d}s = 0$, the PDF of the scalar field collapses to delta function much quicker than the white noise case. We can still calculate the PDF of the scalar field via the PDF of A_0, but the time-independent invariant measure is not available.

5. CONCLUSION AND DISCUSSION

We have studied the long time behavior of an advection-diffusion equation with a general time-varying (including random) shear flow imposing no-flux boundary conditions on channel walls using center manifold theory. Our study extends and improves prior work of [45, 48, 49] to properly incorporate general time variation into the effective theory. Comparisons with full simulations document conditions when this improved approach gives a better approximation and also illustrates situations in which standard homogenization does not perform well on finite timescales. Convergence studies illustrate how the accuracy of the different approximations. Armed with this improved time-varying center manifold theory, we derived new effective equations for random shear flows involving both white in time statistics, as well as more correlated renewing flows. For white in time, these predictions agree with our prior work [32], which forecasts a deterministic effective diffusivity at long times. For the case of renewing flows, less is known, and our

current work also a deterministic effective diffusivity, with new explicit formulae. These theories are demonstrated to be quantitatively accurate through Monte-Carlo simulations. New conditions are derived which guarantee when the random renewing flow generates a larger effective diffusivity than its deterministic analog. Lastly, using the inverse transform method and the effective equations, we derived the invariant measure and investigate its Péclet number dependence.

The future study includes a number of directions. First, in this study, we only considered constant diffusivity. Future immediate areas of exploration include the case with spatial variable-dependent diffusivity or even concentration-dependent diffusivity. A practical example concerns the shear-enhanced diffusion in colloidal suspensions explored in [36]. The nonlinearity in those systems imposes challenges to the traditional method. We expect the center manifold theory could overcome the difficulties. Further, the center manifold theory will apply nicely to study the mixing ability of time-varying flow in a non-flat channel to generalize the conclusion in [57]. Second, the perturbation method presented in the manuscript only works for a decaying scalar field for which energy is localized at zero wavenumbers at long times. We are interested in generalizing the result to plane wave initial data. In this case, since the energy is always localized at a wavenumber isolated from $k = 0$ (set by the initial condition). Hence, the expansion around the zero wavenumbers would not be valid. We expect that the asymptotic expansion is available in the large or small Péclet number limit via the method described in [19, 22]. Additionally, the non-decaying scalar field would exist in the presence of net flux at the boundary or source inside the domain, which is an interesting topic for future study.

6. ACKNOWLEDGEMENTS

7. APPENDIX

7.1. Numerical Method

In this section, we document details of the numerical simulations for equation (1). The computational domain is $x \times y \in [-H, H] \times [0, L]$. When H is large enough, we can assume there is a periodic boundary condition in the x-direction. Since there are non-penetration conditions in the y-direction, we perform the even extension in the y-direction to obtain the periodic condition on the extended domain. Thus, we can use the standard Fourier spectral method to solve the advection-diffusion equation with periodic boundary conditions on the rectangular domain $[-H, H] \times [0, 2L]$. In the dealiasing process at each time step, we apply the all-or-nothing filter with the two-thirds rule to the spectrum, that is, we set the upper one-third of the resolved spectrum to zero (see chapter 11 of the book [17] for details). The typical parameters are $H = 8\pi$, $L = 1$. The grid resolution is 1024×64 before the even extension and 1024×128 after the extension.

The diffusion operator is stiff, which requires a very small time step size for the explicit method to ensure numerical stability. In order to use a larger time step size and improve the efficiency, we adopt the implicit-explicit third-order Runge-Kutta method presented in table 6 in [51]. In our application, we use the explicit Runge-Kutta method to integrate the advection part and use the implicit diagonal Runge-Kutta method to integrate the diffusion term. When the diffusivity is a constant, the diffusion operator is a diagonal matrix in the Fourier space. Thus, the implicit equation can be solved explicitly and efficiently. The implicit-explicit method is as efficient as the explicit method at each iteration while allowing a much larger time step size.

We also present the Butcher tableau of the explicit-implicit Runge-Kutta method in table I here for convenience. Unfortunately, [51] only reported 13-14 significant digits of parameters (α, β, η) which are the key parameters defining the algorithm. That may potentially deteriorate the accuracy of double-precision floating-point based or even higher precision floating-point based algorithms. Hence, we documented the exact value for those parameters, $(\frac{9-\sqrt{57}}{6}, \frac{9-\sqrt{57}}{24}, \frac{-6+\sqrt{57}}{12})$. We also find another two groups of parameters that achieve the same convergence order and ensure the L-stable, $(1/2, 1/8, 0)$ and $(\frac{9+\sqrt{57}}{6}, \frac{9+\sqrt{57}}{24}, \frac{-6-\sqrt{57}}{12})$.

$$
\begin{array}{c|cccc}
0 & 0 & 0 & 0 & 0 \\
0 & 0 & 0 & 0 & 0 \\
1 & 0 & 1 & 0 & 0 \\
\frac{1}{2} & 0 & \frac{1}{4} & \frac{1}{4} & 0 \\
\hline
& 0 & \frac{1}{6} & \frac{1}{6} & \frac{2}{3}
\end{array}
\qquad
\begin{array}{c|cccc}
\alpha & \alpha & 0 & 0 & 0 \\
0 & -\alpha & \alpha & 0 & 0 \\
1 & 0 & 1-\alpha & \alpha & 0 \\
\frac{1}{2} & \beta & \eta & \frac{1}{2}-\beta-\eta-\alpha & \alpha \\
\hline
& 0 & \frac{1}{6} & \frac{1}{6} & \frac{2}{3}
\end{array}
$$

TABLE I: Butcher tableau for the Explicit (left) Implicit (right) L-Stable scheme, (α, β, η) could be $(1/2, 1/8, 0)$, $\left(\frac{9-\sqrt{57}}{6}, \frac{9-\sqrt{57}}{24}, \frac{-6+\sqrt{57}}{12}\right)$ or $\left(\frac{9+\sqrt{57}}{6}, \frac{9+\sqrt{57}}{24}, \frac{-6-\sqrt{57}}{12}\right)$.

7.2. Lists of abbreviations

See table II.

Full Form	Abbreviation
Fisher-Kolmogorov-Petrovskii-Piskunov	FKPP
Ornstein-Uhlenbeck	OU
Partial differential equation	PDE
Probability density function	PDF
Stochastic differential equation	SDE

TABLE II: Lists of abbreviations.

[1] Aiyer, A. K., Subramanian, K., Bhat, P., 2017. Passive scalar mixing and decay at finite correlation times in the batchelor regime. Journal of Fluid Mechanics 824, 785–817.

[2] Aminian, M., Bernardi, F., Camassa, R., Harris, D. M., McLaughlin, R. M., 2016. How boundaries shape chemical delivery in microfluidics. Science 354 (6317), 1252–1256.

[3] Aminian, M., Bernardi, F., Camassa, R., McLaughlin, R. M., 2015. Squaring the circle: Geometric skewness and symmetry breaking for passive scalar transport in ducts and pipes. Physical review letters 115 (15), 154503.

[4] Aminian, M., Camassa, R., McLaughlin, R. M., 2018. Mass distribution and skewness for passive scalar transport in pipes with polygonal and smooth cross sections. Studies in Applied Mathematics 141 (3), 399–417.

[5] Aris, R., 1956. On the dispersion of a solute in a fluid flowing through a tube. Proceedings of the Royal Society of London. Series A. Mathematical and Physical Sciences 235 (1200), 67–77.

[6] Aris, R., 1960. On the dispersion of a solute in pulsating flow through a tube. Proceedings of the Royal Society of London. Series A. Mathematical and Physical Sciences 259 (1298), 370–376.

[7] Aulbach, B., 1982. A reduction principle for nonautonomous differential equations. Archiv der Mathematik 39 (3), 217–232.

[8] Aulbach, B., Wanner, T., 1996. Integral manifolds for Carathéodory type differential equations in Banach spaces. Six lectures on dynamical systems 2.

[9] Aulbach, B., Wanner, T., 1999. Invariant foliations for Carathéodory type differential equations in banach spaces. Advances of Stability Theory at the End of XX Century', Gordon & Breach Publishers. http://citeseerx. ist. psu. edu/viewdoc/-download.

[10] Balakotaiah, V., Chang, H.-C., Smith, F., 1995. Dispersion of chemical solutes in chromatographs and reactors. Philosophical Transactions of the Royal Society of London. Series A: Physical and Engineering Sciences 351 (1695), 39–75.

[11] Bandyopadhyay, S., Mazumder, B., 1999. On contaminant dispersion in unsteady generalised couette flow. International journal of engineering science 37 (11), 1407–1423.

[12] Barik, S., Dalal, D., 2017. On transport coefficients in an oscillatory couette flow with nonlinear chemical decay reactions. Acta Mechanica 228 (7), 2391–2412.

[13] Barik, S., Dalal, D., 2019. Multi-scale analysis for concentration distribution in an oscillatory Couette flow. Proceedings of the Royal Society A 475 (2221), 20180483.

[14] Bhat, P., Subramanian, K., 2015. Fluctuation dynamos at finite correlation times using renewing flows. Journal of Plasma Physics 81 (5).

[15] Blom, M. T., Chmela, E., Oosterbroek, R. E., Tijssen, R., Van Den Berg, A., 2003. On-chip hydrodynamic chromatography separation and detection of nanoparticles and biomolecules. Analytical chemistry 75 (24), 6761–6768.

[16] Bowden, K., 1965. Horizontal mixing in the sea due to a shearing current. Journal of Fluid Mechanics 21 (1), 83–95.

[17] Boyd, J. P., 2001. Chebyshev and Fourier spectral methods. Courier Corporation.

[18] Bronski, J. C., Camassa, R., Lin, Z., McLaughlin, R. M., Scotti, A., 2007. An explicit family of probability measures for passive scalar diffusion in a random flow. Journal of Statistical Physics 128 (4), 927–968.

[19] Bronski, J. C., McLaughlin, R. M., 1997. Scalar intermittency and the ground state of periodic schrödinger equations. Physics of fluids 9 (1), 181–190.

[20] Camassa, R., Ding, L., Kilic, Z., McLaughlin, R. M., 2021. Persisting asymmetry in the probability distribution function for a random advection-diffusion equation in impermeable channels. Physica D: Nonlinear Phenomena, 132930.

[21] Camassa, R., Lin, Z., McLaughlin, R. M., 2010. The exact evolution of the scalar variance in pipe and channel flow. Communications in Mathematical Sciences 8 (2), 601–626.

[22] Camassa, R., McLaughlin, R. M., Viotti, C., 2010. Analysis of passive scalar advection in parallel shear flows: sorting of modes at intermediate time scales. Physics of Fluids 22 (11), 117103.

[23] Carr, J., 2012. Applications of centre manifold theory. Vol. 35. Springer Science & Business Media.

[24] Carr, J., Muncaster, R. G., 1983. The application of centre manifolds to amplitude expansions. i. ordinary differential equations. Journal of differential equations 50 (2), 260–279.

[25] Carr, J., Muncaster, R. G., 1983. The application of centre manifolds to amplitude expansions. ii. infinite dimensional problems. Journal of differential equations 50 (2), 280–288.

[26] Chatwin, P., 1970. The approach to normality of the concentration distribution of a solute in a solvent flowing along a straight pipe. Journal of Fluid Mechanics 43 (2), 321–352.

[27] Chatwin, P., 1975. On the longitudinal dispersion of passive contaminant in oscillatory flows in tubes. Journal of Fluid Mechanics 71 (3), 513–527.

[28] Chatwin, P., Allen, C., 1985. Mathematical models of dispersion in rivers and estuaries. Annual Review of Fluid Mechanics 17 (1), 119–149.

[29] Chu, H. C., Garoff, S., Przybycien, T. M., Tilton, R. D., Khair, A. S., 2019. Dispersion in steady and time-oscillatory two-dimensional flows through a parallel-plate channel. Physics of Fluids 31 (2), 022007.

[30] Chu, H. C., Garoff, S., Tilton, R. D., Khair, A. S., 2020. Dispersion in steady and time-oscillatory flows through an eccentric annulus. AIChE Journal 66 (2), e16831.

[31] Ding, L., Hunt, R., McLaughlin, R. M., Woodie, H., 2021. Enhanced diffusivity and skewness of a diffusing tracer in the presence of an oscillating wall. Research in the Mathematical Sciences 8 (3), 1–29.

[32] Ding, L., McLaughlin, R. M., 2021. Ergodicity and invariant measures for a diffusing passive scalar advected by a random channel shear flow and the connection between the Kraichnan-Majda model and Taylor-Aris dispersion. Physica D: Nonlinear Phenomena, 133118.

[33] Eugene, W., Moshe, Z., 1965. On the relation between ordinary and stochastic differential equations. International Journal of Engineering Science 3 (2), 213–229.

[34] Gill, W., 1967. A note on the solution of transient dispersion problems. Proceedings of the Royal Society of London. Series A. Mathematical and Physical Sciences 298 (1454), 335–339.

[35] Gill, W., Sankarasubramanian, R., 1970. Exact analysis of unsteady convective diffusion. Proceedings of the Royal Society of London. A. Mathematical and Physical Sciences 316 (1526), 341–350.

[36] Griffiths, I., Stone, H. A., 2012. Axial dispersion via shear-enhanced diffusion in colloidal suspensions. EPL (Europhysics Letters) 97 (5), 58005.

[37] Guggenheim, E., 1954. The diffusion coefficient of sodium chloride. Transactions of the Faraday society 50, 1048–1051.

[38] Hairer, M., Pardoux, É., 2015. A Wong-Zakai theorem for stochastic PDEs. Journal of the Mathematical Society of Japan 67 (4), 1551–1604.

[39] Haynes, P. H., Vanneste, J., 2005. What controls the decay of passive scalars in smooth flows? Physics of Fluids 17 (9), 097103.

[40] Jimenez, C., Sullivan, P., 1984. Contaminant dispersion in some time-dependent laminar flows. Journal of Fluid Mechanics 142, 57–77.

[41] Komorowski, T., 2001. Diffusion approximation for the convection-diffusion equation with random drift. Probability theory and related fields 121 (4), 525–550.

[42] Kraichnan, R. H., 1968. Small-scale structure of a scalar field convected by turbulence. The Physics of Fluids 11 (5), 945–953.

[43] Lee, G., Luner, A., Marzuola, J., Harris, D. M., 2021. Dispersion control in pressure-driven flow through bowed rectangular microchannels. Microfluidics and Nanofluidics 25 (4), 1–11.

[44] Majda, A. J., 1993. The random uniform shear layer: an explicit example of turbulent diffusion with broad tail probability distributions. Physics of Fluids A: Fluid Dynamics 5 (8), 1963–1970.

[45] Marbach, S., Alim, K., 2019. Active control of dispersion within a channel with flow and pulsating walls. Physical Review Fluids 4 (11), 114202.

[46] Masri, R., Puelz, C., Riviere, B., 2021. A reduced model for solute transport in compliant blood vessels with arbitrary axial velocity profile. International Journal of Heat and Mass Transfer 176, 121379.

[47] McLaughlin, R. M., Majda, A. J., 1996. An explicit example with non-Gaussian probability distribution for nontrivial scalar mean and fluctuation. Physics of Fluids 8 (2), 536–547.

[48] Mercer, G., Roberts, A., 1990. A centre manifold description of contaminant dispersion in channels with varying flow properties. SIAM Journal on Applied Mathematics 50 (6), 1547–1565.

[49] Mercer, G., Roberts, A., 1994. A complete model of shear dispersion in pipes. Japan journal of industrial and applied mathematics 11 (3), 499–521.

[50] Mukherjee, A., Mazumder, B., 1988. Dispersion of contaminant in oscillatory flows. Acta mechanica 74 (1-4), 107–122.

[51] Pareschi, L., Russo, G., 2005. Implicit–explicit Runge–Kutta schemes and applications to hyperbolic systems with relaxation. Journal of Scientific computing 25 (1), 129–155.

[52] Paul, S., Mazumder, B., 2008. Dispersion in unsteady couette–poiseuille flows. International journal of engineering science 46 (12), 1203–1217.

[53] Renaud, A., Vanneste, J., 2019. Dispersion and reaction in random flows: Single realization versus ensemble average. Physical Review Fluids 4 (12), 124502.

[54] Roberts, A., 1993. The invariant manifold of beam deformations. Journal of elasticity 30 (1), 1–54.

[55] Roberts, A., 1996. Low-dimensional models of thin film fluid dynamics. Physics Letters A 212 (1-2), 63–71.

[56] Roberts, A., Li, Z., 2006. An accurate and comprehensive model of thin fluid flows with inertia on curved substrates. Journal of Fluid Mechanics 553, 33–73.

[57] Rosencrans, S., 1997. Taylor dispersion in curved channels. SIAM Journal on Applied Mathematics 57 (5), 1216–1241.

[58] Salerno, L., Cardillo, G., Camporeale, C., 2020. Aris-Taylor dispersion in the subarachnoid space. Physical Review Fluids 5 (4), 043102.

[59] SMITH, R., 1982. Gaussian approximation for contaminant dispersion. The Quarterly Journal of Mechanics and Applied Mathematics 35 (3), 345–366.

[60] Smith, R., 1987. Diffusion in shear flows made easy: the Taylor limit. Journal of Fluid Mechanics 175, 201–214.

[61] Taylor, G. I., 1953. Dispersion of soluble matter in solvent flowing slowly through a tube. Proceedings of the Royal Society of London. Series A. Mathematical and Physical Sciences 219 (1137), 186–203.

[62] Trojanowicz, M., Kołacińska, K., 2016. Recent advances in flow injection analysis. Analyst 141 (7), 2085–2139.

[63] Van Minh, N., 1993. A reduction principle for topological classification of nonautonomous differential equations. Proceedings of the Royal Society of Edinburgh Section A: Mathematics 123 (4), 621–632.

[64] Vanneste, J., 2006. Intermittency of passive-scalar decay: Strange eigenmodes in random shear flows. Physics of fluids 18 (8), 087108.

[65] Vedel, S., Bruus, H., 2012. Transient Taylor–Aris dispersion for time-dependent flows in straight channels. Journal of fluid mechanics 691, 95–122.

[66] Vedel, S., Hovad, E., Bruus, H., 2014. Time-dependent Taylor–Aris dispersion of an initial point concentration. Journal of fluid mechanics 752, 107–122.

[67] Wang, W., Roberts, A. J., 2013. Self-similarity and attraction in stochastic nonlinear reaction-diffusion systems. SIAM Journal on Applied Dynamical Systems 12 (1), 450–486.

[68] Watson, E., 1983. Diffusion in oscillatory pipe flow. Journal of Fluid Mechanics 133, 233–244.

[69] Watt, S., Roberts, A., 1996. The construction of zonal models of dispersion in channels via matched centre manifolds. The ANZIAM Journal 38 (1), 101–125.

[70] Watt, S. D., Roberts, A. J., 1995. The accurate dynamic modelling of contaminant dispersion in channels. SIAM Journal on Applied Mathematics 55 (4), 1016–1038.

[71] Wong, E., Zakai, M., 1965. On the convergence of ordinary integrals to stochastic integrals. The Annals of Mathematical Statistics 36 (5), 1560–1564.

[72] Wu, Z., Chen, G., 2014. Approach to transverse uniformity of concentration distribution of a solute in a solvent flowing along a straight pipe. Journal of Fluid Mechanics 740, 196–213.

[73] Wu, Z., Fu, X., Wang, G., 2016. On spatial pattern of concentration distribution for Taylor dispersion process. Scientific reports 6 (1), 1–13.

[74] Young, W. a., Jones, S., 1991. Shear dispersion. Physics of Fluids A: Fluid Dynamics 3 (5), 1087–1101.

[75] Zel'Dovich, Y. B., Ruzmaikin, A., Molchanov, S., Sokoloff, D., 1984. Kinematic dynamo problem in a linear velocity field. Journal of Fluid Mechanics 144, 1–11.